

# Aneuploidy can be an evolutionary diversion on the path to adaptation

Ilia Kohanovski<sup>a,b,1</sup>, Martin Pontz<sup>a,1</sup>, Pétra Vande Zande<sup>c</sup>, Anna Selmecki<sup>c</sup>, Orna  
Dahan<sup>d</sup>, Yitzhak Pilpel<sup>d</sup>, Avihu H. Yona<sup>e</sup>, and Yoav Ram<sup>a,\*</sup>

<sup>a</sup>School of Zoology, Faculty of Life Sciences, Tel Aviv University, Tel Aviv, Israel

<sup>b</sup>School of Computer Science, Reichman University, Herzliya, Israel

<sup>c</sup>Department of Microbiology and Immunology, University of Minnesota Medical School, Minneapolis, MN

<sup>d</sup>Department of Molecular Genetics, Weizmann Institute of Science, Rehovot, Israel

<sup>e</sup>Institute of Biochemistry, Food Science and Nutrition, Robert H. Smith Faculty of Agriculture, Food and  
Environment, The Hebrew University of Jerusalem, Israel

<sup>1</sup>These authors contributed equally to this work

\*Corresponding author: yoav@yoavram.com

January 29, 2024

Classifications. Biological Sciences: Evolution, Genetics, Microbiology, Population Biology.

Keywords: whole-chromosome duplication, evolutionary model, adaptive evolution

**Abstract**

Aneuploidy is common in eukaryotes, often leading to decreased fitness. However, evidence from fungi and human tumor cells suggests that specific aneuploidies can be beneficial under stressful conditions and facilitate adaptation. In a previous evolutionary experiment with yeast, populations evolving under heat stress became aneuploid, only to later revert to euploidy after beneficial mutations accumulated. It was therefore suggested that aneuploidy is a “stepping stone” on the path to adaptation. Here, we test this hypothesis. We use Bayesian inference to fit an evolutionary model with both aneuploidy and mutation to the experimental results. We then predict the genotype frequency dynamics during the experiment, demonstrating that most of the evolved euploid population likely did not descend from aneuploid cells, but rather from the euploid wild-type population. Our model shows how the beneficial mutation supply—the product of population size and beneficial mutation rate—determines the evolutionary dynamics: with low supply, much of the evolved population descends from aneuploid cells; but with high supply, beneficial mutations are generated fast enough to outcompete aneuploidy due to its inherent fitness cost. Our results suggest that despite its potential fitness benefits under stress, aneuploidy can be an evolutionary “diversion” rather than a “stepping stone”: it can delay, rather than facilitate, the adaptation of the population, and cells that become aneuploid may leave less descendants compared to cells that remain diploid.

## 34 Introduction

Aneuploidy is an imbalance in the number of chromosomes in the cell: an incorrect karyotype.  
36 Evidence suggests aneuploidy is very common in eukaryotes, e.g. animals (Santaguida and Amon,  
2015; Naylor and van Deursen, 2016; Bakhoun and Landau, 2017), and fungi (Pavelka et al., 2010;  
38 Zhu et al., 2016; Robbins et al., 2017; Todd et al., 2017). Aneuploidy has been implicated in cancer  
formation, progression, and drug resistance (Boveri, 2008; Schvartzman et al., 2010; Santaguida and  
40 Amon, 2015; Rutledge et al., 2016; Ippolito et al., 2021; Lukow et al., 2021). It is also common in  
protozoan pathogens of the *Leishmania* genus, a major global health concern (Mannaert et al., 2012),  
42 and contributes to the emergence of drug resistance (Selmecki et al., 2009) and virulence (Möller  
et al., 2018) in fungal pathogens, which are under-studied (Rodrigues and Albuquerque, 2018), despite  
44 infecting a billion people per year, causing significant morbidity in >150 million and death in >1.5  
million people per year (Selmecki et al., 2009; Rodrigues and Albuquerque, 2018).

46 Experiments with human and mouse embryos found that most germ-line aneuploidies are lethal.  
Aneuploidies are also associated with developmental defects and lethality in other multicellular or-  
48 ganisms (Sheltzer and Amon, 2011). For example, aneuploid mouse embryonic cells grow slower than  
euploid cells (Williams et al., 2008). Similarly, in unicellular eukaryotes growing in benign conditions,  
50 aneuploidy usually leads to slower growth and decreased overall fitness, in part due to proteotoxic  
stress due to increased expression, gene dosage imbalance, and hypo-osmotic-like stress (Niwa et al.,  
52 2006; Torres et al., 2007; Pavelka et al., 2010; Sheltzer and Amon, 2011; Santaguida et al., 2015;  
Kasuga et al., 2016; Zhu et al., 2018; Tsai et al., 2019; Yang et al., 2021; Robinson et al., 2023).

54 However, aneuploidy can be beneficial under stressful conditions due to the wide range of phenotypes  
it can produce, some of which are advantageous (Pavelka et al., 2010; Yang et al., 2021). Indeed, in  
56 a survey of 1,011 yeast strains, aneuploidy has been detected in about 19% (Peter et al., 2018). Thus,  
aneuploidy can lead to rapid adaptation in unicellular eukaryotes (Gerstein et al., 2015; Torres et al.,  
58 2010; Hong and Gresham, 2014; Rancati et al., 2008), as well as to rapid growth of somatic tumour  
cells (Schvartzman et al., 2010; Sheltzer et al., 2017). For example, aneuploidy in *Saccharomyces*  
60 *cerevisiae* facilitates adaptation to a variety of stressful conditions like heat and pH (Yona et al.,  
2012), copper (Covo et al., 2014; Gerstein et al., 2015), salt (Dhar et al., 2011; Robinson et al.,  
62 2023), and nutrient limitation (Dunham et al., 2002; Gresham et al., 2008; Avecilla et al., 2022),  
with similar results in *Candida albicans* (Yang et al., 2021). Importantly, aneuploidy can also lead  
64 to drug resistance in pathogenic fungi such as *C. albicans* (Selmecki et al., 2008, 2010; Gerstein  
and Berman, 2020) and *Cryptococcus neoformans* (Sionov et al., 2010), which cause candidiasis  
66 and meningoencephalitis, respectively. Although we focus here on aneuploidy, a similar phenomena

of adaptation via gene duplication or amplification has been observed in yeast (Lauer et al., 2018),  
68 bacteria (Sonti and Roth, 1989), and DNA viruses (Elde et al., 2012).

Yona et al. (2012) demonstrated experimentally the importance of aneuploidy in adaptive evolution.  
70 They evolved populations of *S. cerevisiae* under strong heat stress. The populations adapted to the  
heat stress within 450 generations, and this adaptation was determined to be due a duplication of  
72 Chromosome III. Later on, after more than 1,500 generations, the populations reverted back to an  
euploid state, while remaining adapted to the heat stress. Aneuploidy was therefore suggested to be a  
74 transient adaptive solution, because it can rapidly appear and take over the population under stressful  
conditions, and can then be rapidly lost when the cost of aneuploidy outweighs its benefit—after the  
76 stress is removed, or after refined beneficial mutations appear and fix (Yona et al., 2012). Furthermore,  
78 it has been suggested that aneuploidy is an evolutionary “stepping stone” that facilitates future  
adaptation by genetic mutations, which require more time to evolve (Yona et al., 2012, 2015).

Here, we test the hypothesis that aneuploidy is an evolutionary “stepping stone” that facilitates adaptive  
80 evolution by genetic mutations (Yona et al., 2012). We develop an evolutionary genetic model and fit  
it to the experimental results of Yona et al. (2012) to predict the genotype frequency dynamics in the  
82 experimental populations, thereby estimating the frequency of evolved euploid cells that descended  
from aneuploid cells. Our results show that although aneuploidy reached high frequencies in the  
84 experimental populations, the majority of cells in the evolved euploid population likely did not  
descend from aneuploid cells, but rather directly from wild-type euploid cells. These suggests that at  
86 the lineage level, aneuploidy may be an “evolutionary diversion”, rather than a “stepping stone”, on  
the path to adaptation.

## 88 **Results**

In the heat-stress experiment of Yona et al. (2012), four populations of *S. cerevisiae* evolved under  
90 39°C. Aneuploidy reached high frequency (>95%) in all four experimental repetitions in the first 450  
generations. Two of the repetitions, marked *H2* and *H4*, carried no large-scale duplications other  
92 than a Chromosome III trisomy. These two repetitions continued to evolve under the same conditions,  
wherein aneuploidy was eliminated by generation 1,700 and 2,350 in *H4* and *H2*, respectively.

94 **Evolutionary genetic model.** To explore the dynamics during the evolutionary experiments, we  
developed an evolutionary genetic model, fitted the model to empirical data, and used it to predict the  
96 genotype frequency dynamics, or specifically, the fraction of the evolved euploid population descended  
from aneuploid cells.

98 The model includes the effects of natural selection, genetic drift, aneuploidy, and mutation (i.e., other  
 99 genetic variants), and follows a population of cells characterized by their genotype: euploid wild-  
 100 type,  $2n$ , is the ancestral diploid genotype; euploid mutant,  $2n^*$ , has a diploid karyotype and a single  
 101 beneficial mutation; aneuploid wild-type,  $2n + 1$ , has an extra chromosome due to a chromosome  
 102 duplication event; and aneuploid mutant,  $2n + 1^*$ , has an extra chromosome (like  $2n + 1$ ) and a  
 103 beneficial mutation (like  $2n^*$ ). Note that ‘mutation’ here refers to point mutations and other genetic  
 104 variants unrelated to aneuploidy. Fitness values of the different genotypes are denoted by  $w_{2n}$ ,  $w_{2n^*}$ ,  
 105  $w_{2n+1}$ , and  $w_{2n+1^*}$ , and the rate of mutation and aneuploidy are denoted by  $\mu$  and  $\delta$ , respectively. See  
 106 Figure 1 for an illustration of the model.

We fitted this model to the experimental results(Yona et al., 2012)–time for fixation (frequency >95%)  
 107 and for loss (frequency <5%) of aneuploidy–using approximate Bayesian computation with sequential  
 108 Monte Carlo (ABC-SMC) (Sisson et al., 2007), thereby inferring the model parameters: rates of  
 109 aneuploidy (i.e., mis-segregation, non-disjunction) and mutation and the fitness of all genotypes.  
 We then sampled posterior predictions for the genotype frequency dynamics using the estimated  
 110 parameter values and compared different versions of the model to test additional hypotheses about the  
 111 evolutionary process.

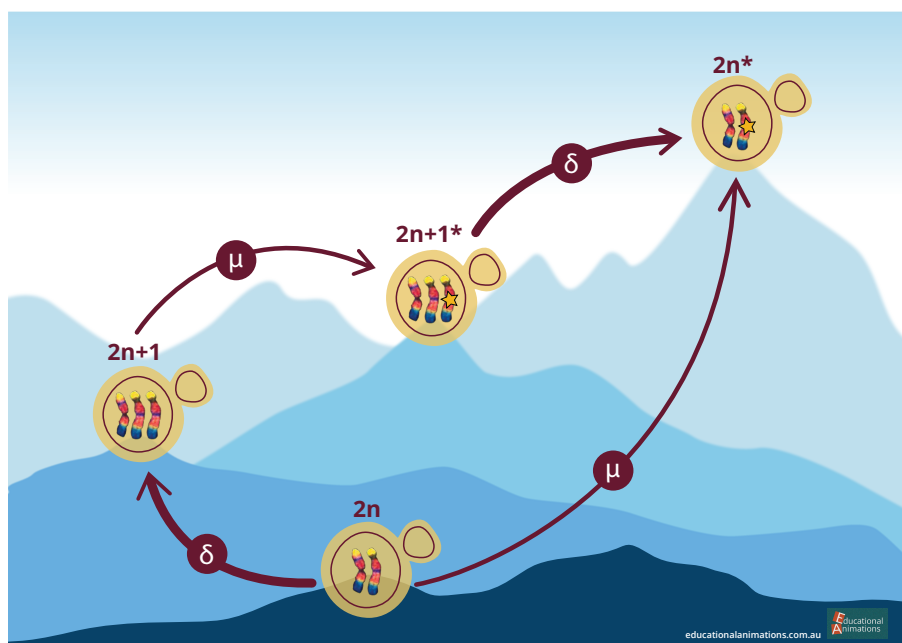


**Figure 1: Model Illustration.** There are four genotypes in our model: euploid wild-type,  $2n$ ; euploid mutant,  $2n^*$ ; aneuploid wild-type,  $2n + 1$ ; and aneuploid mutant,  $2n + 1^*$ . Overall there are two possible trajectories from  $2n$  to  $2n^*$ . Arrows denote transitions between genotypes, with transition rates  $\mu$  for the beneficial mutation rate and  $\delta$  for the aneuploidy rate. Elevation differences illustrate the expected, rather than the assumed, fitness differences between the genotypes.

114 **Estimated rates and fitness effects of aneuploidy and mutation.** We inferred the posterior distribution  
115 of model parameters (Figure 2). We report parameter estimates using the MAP (maximum a  
116 posteriori) and providing the 50% HDI (highest density interval) in square brackets. See Supplementary Material for sensitivity analysis.

118 The estimated beneficial mutation rate is  $\mu = 2.965 \cdot 10^{-6}$  [ $2.718 \cdot 10^{-7} - 3.589 \cdot 10^{-6}$ ] per genome per generation (that is, roughly 3 out of  $10^6$  cell divisions produce a mutant cell with a fitness advantage).  
120 From the literature, the mutation rate per base pair is roughly  $2 - 3 \cdot 10^{-10}$  (Zhu et al., 2014; Lynch et al., 2008), but it may be higher under heat stress, as several stresses (Heidenreich, 2007), including  
122 heat (Huang et al., 2018), may cause hypermutation in yeast. If we assume a 10-fold increase over the mutation rate reported in the literature, then the estimated beneficial mutation rate can be explained  
124 by a genomic target size of 1,000 base pairs (that is, 1,000 base pairs across the genome in which a mutation would provide a fitness advantage):  $3 \cdot 10^{-10} \times 10 \times 1,000 = 3 \cdot 10^{-6}$ . Supporting this, Jarolim et al. (2013) found 279 genes that contributed to survival after a sudden shift from  $30^\circ\text{C}$  to  $50^\circ\text{C}$ , and Flynn et al. (2020) used a deep mutational scan of a single protein, Hsp90, to find 465 amino-acid variants (out of 14,160) that significantly increased growth rate in  $37^\circ\text{C}$ . Furthermore, Yona et al. (2012) found at least 10 genes on Chromosome III that increased heat tolerance when over-expressed.  
130 Assuming that other chromosomes also have a similar number of heat-tolerance genes (and even more, as Chromosome III is one of the smallest chromosomes (Gilchrist and Stelkens, 2019)), we estimate  
132 a total of 160 heat-tolerance genes in the genome. Indeed, mutations were found in 97 genes in an evolutionary experiment with yeast under heat stress (Huang et al., 2018). Thus, to get a genomic  
134 target size of 1,000, it is enough that the average gene target size (number of base pairs in a gene in which a mutation is beneficial) is 6.25 base pairs. For example, Kohn and Anderson (2014) found a  
136 target size of 11 in a proton exporter gene (*PMA1*) that contributes to high-salt adaptation.

The estimated rate of aneuploidy (i.e., mis-segregation, non-disjunction),  $\delta = 1.72 \cdot 10^{-3}$  [ $1.47 \cdot 10^{-3} - 2.786 \cdot 10^{-3}$ ] is higher than in previous studies: for Chromosome III in diploid *S. cerevisiae*, Zhu et al. (2014) estimated  $6.7 \cdot 10^{-6}$  chromosome gain events per generation, and Kumaran et al. (2013) estimate  $3.0 \cdot 10^{-5} - 4.3 \cdot 10^{-5}$  chromosome loss events per generation (95% confidence interval). However, this difference may be partly explained by an increased rate of aneuploidy during heat stress:  
142 heat shock can increase the rate of chromosome fragment loss by 2-3 orders of magnitude (Chen, Bradford, Seidel and Li, 2012).

144 The estimated fitness values are  $w_{2n+1} = 1.022$  [ $1.021 - 1.023$ ],  $w_{2n+1^*} = 1.025$  [ $1.024 - 1.026$ ],  
146  $w_{2n^*} = 1.028$  [ $1.026 - 1.029$ ], all relative to the fitness of  $2n$ , which is set to  $w_{2n} = 1$ . If we allow for transitions (mutation, chromosome loss and gain) to less-fit genotypes (e.g.,  $2n^*$  to  $2n + 1^*$ ), then we

infer similar but slightly different values, see Supplementary Material.

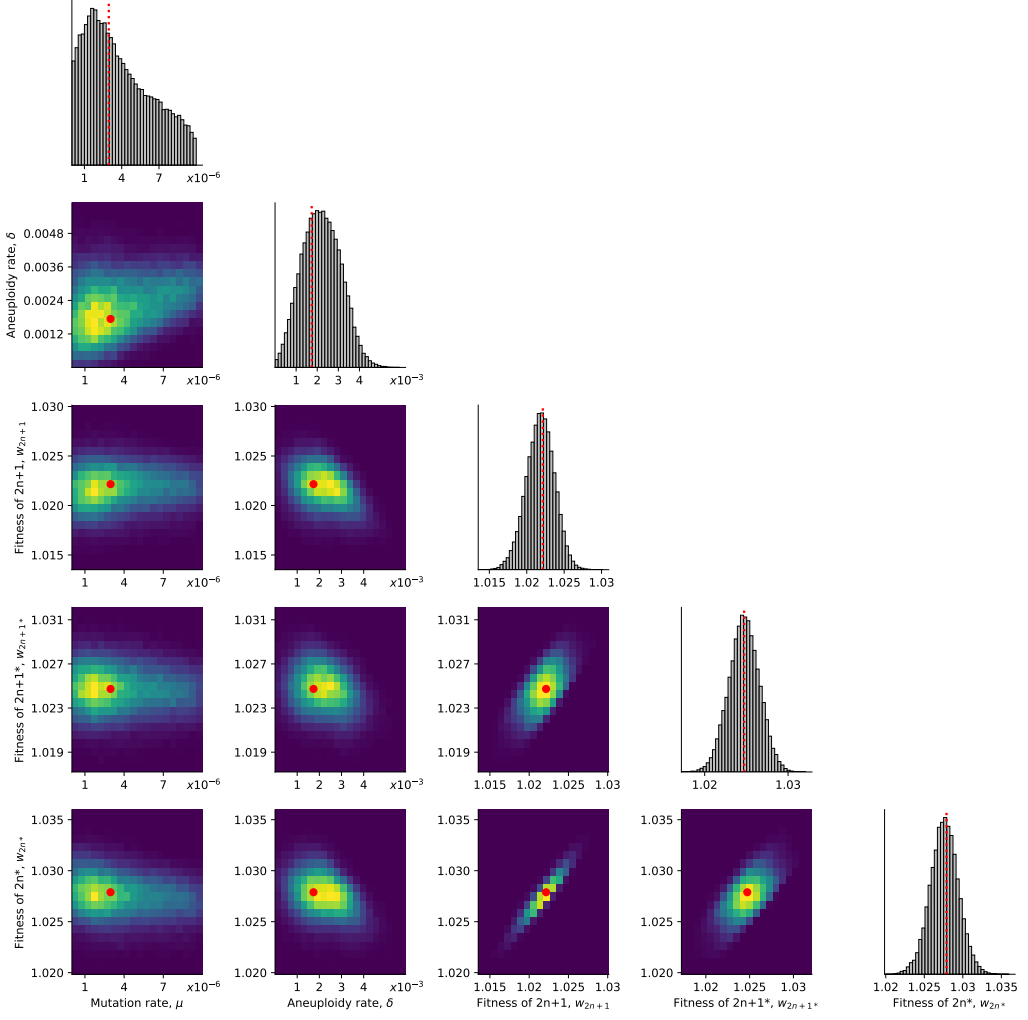


**Figure 2: Posterior distribution of model parameters.** On the diagonal, the marginal posterior distribution of each model parameter. Below the diagonal, the joint posterior distribution of pairs of model parameters (dark purple and bright yellow for low and high density, respectively). Red markers and orange lines for the joint MAP estimate (which may differ from the marginal MAP, as the marginal distribution integrates over all other parameters).

- 148 **Model comparison and goodness-of-fit.** To assess the fit of our model to the data, we use posterior  
149 predictive checks, in which we simulate the frequency dynamics using MAP parameter estimates and  
150 compare them to the data. Our model fits the data well:  $2n^*$  fixed in 63% of simulations by generation  
1,700 and in 100% of simulations by generation 2,350 (Figure 3).
- 152 However, a model without aneuploidy (where the aneuploidy rate is fixed at zero,  $\delta = 0$ ), fails to  
153 explain the experimental observations (Figure 3). The estimated mutation rate without aneuploidy is  
154  $\mu = 7.98 \cdot 10^{-9}$  [ $7.906 \cdot 10^{-9} - 8.138 \cdot 10^{-9}$ ], much lower compared to a model with aneuploidy. The  
155 fitness of the mutant is also much lower at  $w_{2n^*} = 1.013$  [ $1.012 - 1.013$ ]. This is because, without

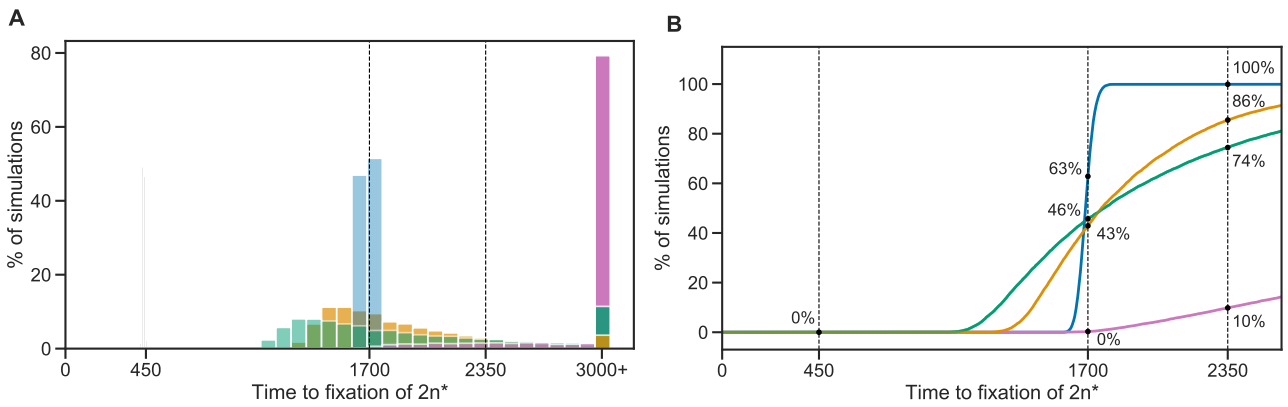


**Figure 3: Model fit with and without aneuploidy.** The distribution of time to fixation of  $2n^*$  (i.e., adaptation time) in 10,000 simulations using MAP parameters of the model with beneficial aneuploidy (blue;  $\delta > 0$ ,  $w_{2n} < w_{2n+1} < w_{2n+1^*} < w_{2n^*}$ ) compared to alternative models: a model with the same parameter values but without aneuploidy (gray,  $\delta = 0$ , concentrated at  $t = 450$ ); a model fitted to the data assuming no aneuploidy (green,  $\delta = 0$ ); a model fitted to the data assuming neutral aneuploidy (yellow,  $\delta > 0$ ,  $w_{2n+1} = w_{2n}$ ,  $w_{2n+1^*} = w_{2n^*}$ ); and a model with beneficial aneuploidy and an extended prior distribution (pink). In the experiment by Yona et al. (2012), one population lost aneuploidy by generation 1,700 and another by generation 2,350 (dashed lines) but not before generation 450. Thus, the blue distribution has a better fit compared to the other distributions (the gray distribution has a particularly poor fit). The MAP likelihood (eq. (4)) is 0.84, 0.78, 0.67, and 0.14 for the models represented by blue, yellow, green, and pink distributions, respectively. **(A)** Histogram of the time to fixation of  $2n^*$ . The last bin contains all values equal or greater than 3,000. **(B)** Cumulative distribution of the time to fixation.

156 aneuploidy, a high mutation rate or fitness effect will lead to faster appearance and fixation of  $2n^*$  than  
in the experimental observations.

158 We also checked a model in which aneuploidy occurs but is adaptively neutral compared to the wild-  
type, that is,  $w_{2n+1} = w_{2n}$  and  $w_{2n+1^*} = w_{2n^*}$  but  $\delta > 0$ . This model fits the data better than the model  
160 with no aneuploidy (in which  $\delta = 0$ ), but worse than a model with positive selection for aneuploidy,  
in which  $w_{2n} < w_{2n+1} < w_{2n+1^*} < w_{2n^*}$  (Figure 3).

162 **Model predictions of genotype frequency dynamics.** We simulated 50 replicate genotype fre-  
quency dynamics using the MAP estimate parameters. Figure 4A shows the simulated frequencies of  
164 the four genotypes ( $2n$ ,  $2n + 1$ ,  $2n + 1^*$  and  $2n^*$ ), as well as the frequencies of  $2n^*$  cells that arose from  
either  $2n + 1$  cells via a sequences of mutation and chromosome loss events ( $2n_A^*$ ), or directly from  
166  $2n$  cells via a mutation event ( $2n_M^*$ ). We find that  $2n + 1^*$  never reaches substantial frequency as it  
is quickly replaced by  $2n^*$  in a process similar to *stochastic tunneling* (Iwasa et al., 2004; Komarova

168 et al., 2003).

To test the hypothesis that aneuploidy facilitates adaptation, we estimated  $F_A$ , the expected frequency  
170 of  $2n^*$  that arose from  $2n + 1$ , computed as the average frequency of such  $2n_A^*$  cells at the end of  
simulations using the MAP estimate parameters. Surprisingly, we observe that the majority of  $2n^*$   
172 cells are  $2n_M^*$ , a product of a direct mutation in  $2n$  cells, rather than descending from  $2n + 1$  cells  
( $F_A^{MAP} = 0.106$ , average end point of 50 purple lines in Figure 4A). This is despite the fact that the  
174  $2n + 1$  genotype reaches high frequencies in the population (at least 0.98, Figure 4A).

This result is not unique to the MAP parameter estimate. We simulated genotype frequency dynamics  
176 using parameter samples from the posterior distribution, and computed the posterior distribution of  
 $F_A$  (Figure 4B). The posterior mode  $F_A$  was just 0.147 [0.0154-0.370 95% CI] and only in 489 of  
178 100,000 posterior samples (0.489%)  $F_A$  was larger than 0.5 (see Supporting Material for results when  
transitions to less-fit genotypes are allowed, such as  $2n^*$  to  $2n + 1^*$ ). Thus, if we sample a random  
180 cell from the evolved  $2n^*$  population, it is more likely to have descended directly from an euploid  
cell than from an aneuploid cell. The probability of  $2n^*$  descending from  $2n + 1$  ( $F_A$ ) increases  
182 with the aneuploidy rate,  $\delta$ , and decreases with both the population size  $N$  and the mutation rate,  $\mu$   
(Figure 4C,D). In some cases it can also be affected by the fitness parameters (Figure S10).

184 **Genetic instability in aneuploid cells.** It has been suggested that aneuploidy increases genomic  
instability: Sheltzer et al. (2011) have demonstrated a fold increase of between 2.2 and 7.1 in the  
186 mutation rate of disomic yeast (rather than trisomic yeast, the focus of our analysis). Therefore, we  
inferred model parameters under the assumption that the mutation rate increases in aneuploid cells by a  
188 factor  $\tau = 1, 33/32$  (due to an additional chromosome), 2, 5, 10, or 100 (due to genetic instability). We  
found that the posterior distribution was similar for  $\tau = 1, 33/32, 2$ , and 5 (Figure S4). Furthermore,  
190 we computed the WAIC, a criterion for model selection (Methods). The WAIC values were similar  
for all  $\tau$  values (Table S1).

192 Assuming a strong increase of the mutation rate in aneuploid cells, i.e.  $\tau = 100$ , the inferred a  
mutation rate was  $\mu = 4.094 \cdot 10^{-7}$  [ $6.252 \cdot 10^{-8} - 6.046 \cdot 10^{-7}$ ]), and the inferred aneuploidy rate  
194 that was  $\delta = 0.744 \cdot 10^{-3}$  [ $0.506 \cdot 10^{-3} - 1.827 \cdot 10^{-3}$ ]. Compared to inference made assuming no  
effect of aneuploidy on the mutation rate, these rates were about 7-8-fold and 2-3-fold lower for  $\mu$  and  
196  $\delta$ , respectively. Assuming  $\tau = 10$ , the inferred a mutation rate was only slightly lower compared to  
 $\tau = 1$  ( $\mu = 1.67 \cdot 10^{-6}$  [ $2.836 \cdot 10^{-8} - 2.245 \cdot 10^{-6}$ ]).

198 Therefore, we do not find evidence of an increase in mutation rate in aneuploid cells. This may be

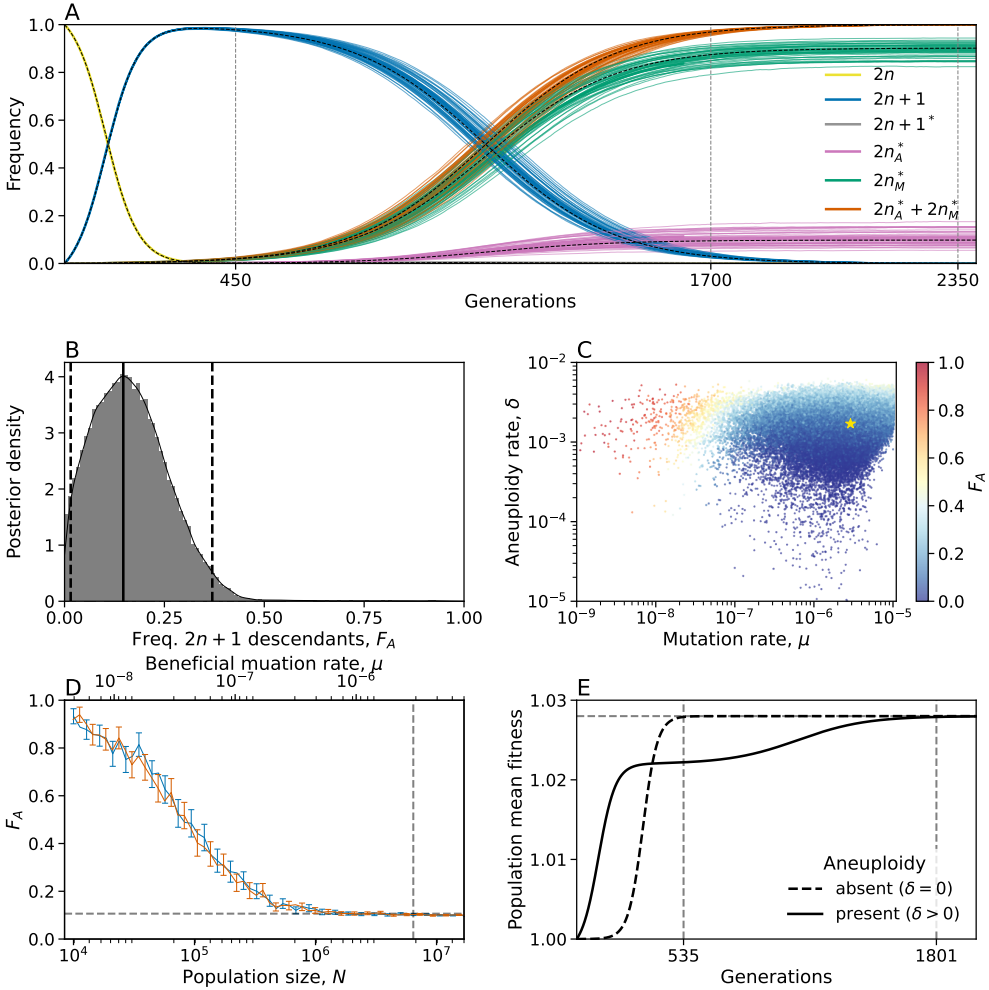


**Figure 4: Predicted frequency of aneuploid-descended cells.** **(A)** Posterior predicted genotype frequencies over time, including the source of  $2n^*$ :  $2n_A^*$  arose from  $2n + 1$ , whereas  $2n_M^*$  arose directly from  $2n$ . Colored curves are 50 simulations using the MAP estimate parameters. Black dashed curves are the expected genotype frequencies without genetic drift (from a deterministic model). See Figure S9 for log-log scale, in which the sequence of events is easier to observe. **(B)** Posterior distribution of  $F_A$ , the expected frequency of  $2n^*$  cells descended from  $2n + 1$  cells, computed as the average frequency at the end of 100 simulations for 100,000 samples from the parameter posterior distribution. Solid and dashed lines show the mode and 95% CI. **(C)**  $F_A$  values (color coded) from panel B, with their corresponding mutation rate  $\mu$  on x-axis and aneuploidy rate  $\delta$  on the y-axis. Yellow star shows the MAP estimate. See also Figure S10. **(D)**  $F_A$  as a function of the population size ( $N$ , bottom x-axis) and the beneficial mutation rate ( $\mu$ , top x-axis) in posterior predictions with MAP parameters. Markers show  $F_A$  in 250 simulations per population size or mutation rate value. Error bars show mean  $F_A$  with 95% CI (bootstrap,  $n = 10,000$ ). Blue and red bars for varying population size and mutation rate, respectively. Vertical dashed line for population size in the experiment,  $6.425 \cdot 10^6$ , and the MAP mutation rate,  $2.965 \cdot 10^{-6}$ . Horizontal line for  $F_A^{MAP} = 0.106$ . **(E)** Population mean fitness in a model without drift using MAP estimate parameters. Solid lines for mean fitness with aneuploidy ( $\delta > 0$ ), where the population reaches adaptation (mean fitness at 99.99% of maximum value) at generation 1,802. Dashed lines for mean fitness without aneuploidy ( $\delta = 0$ ), where the population adapts much earlier, at generation 535.

because, unless the increase is strong ( $\tau \geq 10$ ), it does not seem to affect our inference; or because  
200 Chromosome III is one of the smallest chromosomes (Gilchrist and Stelkens, 2019). We also checked  
the differences in genotype frequency dynamics for different  $\tau$  values. We observe  $\tau = 100$  could be  
202 distinguished if accurate data was available for the waiting time until the frequency of  $2n$  to decrease  
below 95% (Figure S5A) or for waiting time for the frequency of  $2n + 1$  to either reach or go below  
204 95% (Figure S5B).

Similarly, we did not find evidence for an increase in the rate of chromosome loss in aneuploid  
206 cells (Sheltzer et al., 2011), probably due to lack of statistical power. Nevertheless, increasing the rate  
of chromosome loss (transitions from  $2n + 1^*$  to  $2n^*$ ) without increasing the rate of chromosome gain  
208 (transitions from  $2n$  to  $2n + 1$ ) increases  $F_A$  (Figure S11B), but not to the same extent as increasing  
the rate of chromosome gain (Figure S10). In contrast, increasing the mutation rate in aneuploid cells  
210 can have a marked effect on the dynamics: when using the MAP parameter estimates,  $F_A$  increases  
from 0.1 to 0.52 when the mutation rate in aneuploid cells increases 10-fold (Figure S11C).

## 212 Discussion

In a study on the role of chromosome duplication in adaptive evolution, Yona et al. (2012) found that  
214 a Chromosome III trisomy was acquired by *S. cerevisiae* populations evolving under heat stress, only  
to be later replaced by euploid mutant cells that carry "refined" solutions to the stress. Additionally,  
216 such a replacement also occurred when they initiated evolutionary experiments with a population in  
which all cells carry a Chromosome III trisomy. They hypothesized that aneuploidy is a "useful yet  
218 short-lived intermediate that facilitates further adaptation", suggesting that the euploid mutant cells  
evolved by heat-resistance mutations in aneuploid cells followed by reversion of trisomy due to a  
220 chromosome loss event.

We developed an evolutionary genetic model of adaptive evolution by aneuploidy and mutation  
222 (Figure 1), fitted it to the experimental results of Yona et al. (2012), and used it to predict the genotype  
frequency dynamics. The model predicted that only about 10-15% of the evolved euploid population  
224 descended from aneuploid cells by acquiring a mutation and losing the extra chromosome—that is,  
the majority of the euploid population are not descended from aneuploid cells, but rather are direct  
226 descendants of the ancestral wild-type population (Figure 4).

This happens despite aneuploidy reaching a high frequency in the population (>95%). Conventional  
228 wisdom might suggest that once the aneuploid genotype  $2n + 1$  reaches high frequency, it will have a  
better chance at producing "refined" solutions via mutations, and its descendants will come to dominate

230 the population: the frequency of  $2n_A^*$  (which arises from  $2n + 1^*$ ) will be higher than the frequency of  
231  $2n_M^*$  (which arises directly from  $2n$ ).  
232 So how does  $2n_M^*$  prevail? Initially, the supply rates of  $2n + 1$  and  $2n_M^*$  are  $N\delta \approx 11,000$  and  $N\mu \approx 19$ ,  
233 respectively (assuming MAP parameter estimates). Therefore, both genotypes are expected to appear  
234 immediately at the beginning of the experiment (Figure S9). However,  $2n + 1$  appears at a much higher  
235 frequency as  $\delta \gg \mu$  by 2-3 orders of magnitude. After they first appear,  $2n_M^*$  has higher fitness. But  
236 as long as the frequency of  $2n$  is high, the supply rate of  $2n + 1$  is higher than that of  $2n_M^*$ , again due to  
237  $\delta \gg \mu$ . However, supply rates of both genotypes decreases with the frequency of  $2n$ . Therefore, when  
238 the latter decreases, mainly due to the increase in the frequency of  $2n + 1$ , both supply rates diminish.  
At this stage, the higher fitness of  $2n_M^*$  comes into play and it starts to take over the population, which  
240 is mainly composed of  $2n + 1$ . For the aneuploid lineage to compete with the mutant lineage, it  
241 must produce  $2n_A^*$  via a mutation followed by chromosome loss. Although this is a stochastic process  
242 (due to drift), our results show that the time until  $2n_A^*$  reaches a frequency of 0.1% is roughly 450  
generations, without much variation (intersection of purple lines and vertical dashed line in Figure S9).  
244 However, by that time  $2n_M^*$  is already at a roughly 10-fold higher frequency (1.86%), and since both  
mutants have the same fitness, their relative frequency remains roughly the same until the end of the  
246 experiment.

**Predictions for small populations and low mutation rates.** We examined the effect of the popula-  
248 tion size,  $N$ , and the beneficial mutation rate,  $\mu$ , on the frequency of  $2n + 1$  descendants in the evolved  
population,  $F_A$ . We found that  $F_A$  is expected to decrease as the population size or mutation rate  
250 increase (Figure 4D), ranging from >90% when the population size is 10,000 or the mutation rate is  
 $6 \cdot 10^{-9}$ , to about 10% when the population size is above 1,000,000 (less than the experimental popu-  
252 lation size, which was 6,425,000) or the mutation rate is above  $2 \cdot 10^{-6}$  (less than the inferred mutation  
rate, which is  $2.965 \cdot 10^{-6}$ ). Thus, our model provides a testable prediction: if the experiment was  
254 repeated under a lower population size (via stronger daily dilutions or in a smaller volume) or a lower  
mutation rate (via a non-mutagenic stress or stress with a smaller target size such as drug resistance),  
256 then the fraction of the population descending from aneuploid cells would be much higher.

**Aneuploidy delays rather than facilitates adaptation.** An additional interesting result of our  
258 study is that aneuploidy increases, rather than decreases, the adaptation time (Figure 4E). This  
happens despite the fact that the mean fitness initially increases faster in the presence of aneuploidy  
260 (Figure 4E). Aneuploidy increases adaptation time because once  $2n + 1$  is common, selection for the  
mutant strain ( $2n + 1^*$  or  $2n^*$ ) is weaker compared to when  $2n^*$  competes directly with  $2n$ . This is an

262 interesting example of clonal interference (Good et al., 2012) but between fast and slow mutational  
263 processes (Kronholm and Collins, 2016).

264 **Rate and fitness effect of aneuploidy and mutation.** We inferred the rates of aneuploidy and  
265 mutation and their effects on fitness. We estimate that the aneuploidy rate (i.e., number of chromosome  
266 gains per generation) is  $1.7 \cdot 10^{-3}$ , higher than a previous estimate of  $6.7 \cdot 10^{-6}$  (Zhu et al., 2016). This  
267 may be due to genetic instability caused by heat stress (Chen, Bradford, Seidel and Li, 2012), but we  
268 note that there is a general scarcity of empirical data on aneuploidy rates. In addition, we did not find  
269 evidence for increased mutation rates in aneuploid cells. Previous empirical studies have suggested  
270 that genetic instability (e.g., elevated mutation rates) in aneuploid cells is due to stress associated  
271 with the aneuploid state (Bouchonville et al., 2009; Chen, Rubinstein and Li, 2012; Zhu et al., 2012;  
272 Ippolito et al., 2021). However, in the experiment of Yona et al. (2012), both the wild-type and the  
273 aneuploid were under heat stress, which may explain why we didn't find evidence for an increased  
274 mutation rate specifically in aneuploid cells.

275 **Effect of ploidy.** The evolutionary dynamics may change in haploid yeast, in which aneuploidy  
276 results in a second, rather than third, chromosome copy. For example, it has been demonstrated that  
277 drug resistance mainly evolves via recessive mutations and aneuploidy in haploid yeast (Soncini et al.,  
278 2020), whereas in diploid yeast it evolves via dominant mutations, aneuploidy, and gene/segmental  
279 duplications (Barney et al., 2021). Thus, the second chromosome copy of disomic yeast may facilitate  
280 further adaptation via duplications, rearrangements, and increased mutational tolerance (Avecilla  
281 et al., 2023), while decreasing the chance for adaptation via recessive mutations. Future models and  
282 experiments can consider how ploidy and other genomic contexts affect the role of aneuploidy in  
283 adaptive evolution.

284 **Conclusions.** Here, we tested the hypothesis that aneuploid cells are an evolutionary “stepping  
285 stone”, or adaptive intermediate, between wild-type euploid cells and mutant euploid cells in the  
286 evolutionary experiment of Yona et al. (2012). Our results suggest that, although it seems the  
287 population goes from euploid to aneuploid and back, this is not the case at the individual level.  
288 We estimate that only about 10-15% of the euploid cells descended from aneuploid cells, whereas  
289 the rest are direct descendants of the wild-type euploid cells. Thus, aneuploidy can delay, rather  
290 than accelerate, adaptation, and cells that become aneuploid may leave less descendants than cells  
291 that remain euploid. This surprising result reinforces the importance of mathematical models when  
292 interpreting evolutionary dynamics. Moreover, our study emphasizes the unintuitive outcomes of

clonal interference between mechanisms for generation of variation that differ in their rate of formation  
294 and distribution of fitness effects, including mutation, copy number variation, horizontal gene transfer,  
and epigenetic modifications.

## 296 Models and Methods

**Evolutionary genetic model.** We model the evolution of a population of cells using a Wright-Fisher model (Otto and Day, 2007), assuming a constant effective population size  $N$ , non-overlapping generations, and including the effects of natural selection, genetic drift, aneuploidy, and mutation. We focus on beneficial genetic modifications, neglecting the effects of deleterious and neutral mutations or karyotypic changes. The model allows for a single aneuploid karyotype (e.g., Chromosome III duplication) and a single mutation to accumulate in the genotype. Thus, the model follows four genotypes (Figure 1): euploid wild-type,  $2n$ , the initial genotype; euploid mutant,  $2n^*$ , with the standard karyotype and a single beneficial mutation; aneuploid wild-type,  $2n + 1$ , with an extra chromosome, i.e., following chromosome duplication; and aneuploid mutant,  $2n + 1^*$ , with an extra chromosome and a beneficial mutation.

Transitions between the genotypes occur as follows (Figure 1): Beneficial mutations from  $2n$  to  $2n^*$  and from  $2n+1$  to  $2n+1^*$  occur with probability  $\mu$ , the mutation rate. We neglect back-mutations (i.e., from  $2n^*$  to  $2n$  and from  $2n + 1^*$  to  $2n + 1$ ). Aneuploidy is formed by chromosome mis-segregation, so that cells transition from  $2n$  to  $2n + 1$  and from  $2n + 1^*$  to  $2n^*$  with probability  $\delta$ , the aneuploidy rate. That is, we assume chromosomes are gained and lost at the same rate, and we neglect events that form a less-fit genotype (i.e.,  $2n + 1$  to  $2n$  and  $2n^*$  to  $2n + 1^*$ ). A model that assumes an increased rate of chromosome loss in aneuploid cells (as in Sheltzer et al. (2011)) did not perform well, probably due to lack of statistical power, and was abandoned.

In the experiment by Yona et al. (2012), the population was grown every day from  $1.6 \cdot 10^6$  cells until reaching stationary phase and then diluted 1:120. Thus, we set the population size to  $N = 6.425 \cdot 10^6$ , the harmonic mean of  $\{2^k \cdot 1.6 \cdot 10^6\}_{k=0}^7$  (Crow and Kimura, 1970). The initial population has  $N$  cells with genotype  $2n$ . The effect of natural selection on the frequency  $f_i$  of genotype  $i = 2n, 2n+1, 2n+1^*$ , or  $2n^*$  is given by

$$320 \quad f_i^s = \frac{f_i w_i}{\bar{w}} , \quad (1)$$

where  $w_i$  is the fitness of genotype  $i$  and  $\bar{w} = \sum_j f_j w_j$  is the population mean fitness. The effect of

322 mutation and aneuploidy on genotype frequencies is given by

$$\begin{aligned} f_{2n}^m &= (1 - \delta - \mu) f_{2n}^s, \\ f_{2n+1}^m &= \delta f_{2n}^s + (1 - \mu) f_{2n+1}^s, \\ f_{2n+1^*}^m &= \mu f_{2n+1}^s + (1 - \delta) f_{2n+1^*}^s, \\ f_{2n^*}^m &= \mu f_{2n}^s + \delta f_{2n+1^*}^s + f_{2n^*}^s. \end{aligned} \tag{2}$$

324 Finally, random genetic drift is modeled using a multinomial distribution (Otto and Day, 2007),

$$\mathbf{f}' \sim \frac{1}{N} \cdot \text{Mult}(N, \mathbf{f}^m), \tag{3}$$

326 where  $\mathbf{f}^m = (f_{2n}^m, f_{2n+1}^m, f_{2n+1^*}^m, f_{2n^*}^m)$  are the frequencies of the genotypes after mutation and  
aneuploidy,  $\mathbf{f}'$  are the genotype frequencies in the next generation, and  $\text{Mult}(N, \mathbf{f})$  is a multinomial  
328 distribution parameterized by the population size  $N$  and the genotype frequencies  $\mathbf{f}$ . Overall, the change  
in genotype frequencies from one generation to the next is given by the transformation  $f_i \rightarrow f'_i$ .

330 **Empirical data for model inference.** We use the results of evolutionary experiments reported by  
Yona et al. (2012). In their heat-stress experiment, four populations of *S. cerevisiae* evolved under  
332 39°C. Aneuploidy fixed (frequency >95%) in all four population in the first 450 generations. Hereafter,  
fixation or elimination of a genotype by generation  $t$  means that more than 95% or less than 5% of the  
334 population carry the genotype at generation  $t$ , and possibly earlier. In the original analysis of Yona  
et al. (2012), samples were routinely extracted from the evolving populations and tested for indication  
336 of heat-shock tolerance. The first generation in which such indication was found was generation 200.  
Therefore, we determine that aneuploidy did not reach high frequency before generation 200. The  
338 experiment continued with two populations, in which aneuploidy was eliminated by generation 1,700  
and 2,350 while still under the same conditions of elevated heat (39°C).

340 **Likelihood function.** Because our model, just like the Wright-Fisher model, is non-linear and  
stochastic, computing the distribution of fixation time  $T(g)$  of genotype  $g$  for use in the likelihood  
342 function is intractable (it is even hard to use a diffusion-equation approximation due to the model having  
multiple genotypes, rather than just two). We overcome this problem by approximating the likelihood  
344 using simulations. We simulate 1,000 experiments per parameter vector  $\theta = (\mu, \delta, s, b, c)$ , resulting

in a set of simulated observations  $\tilde{\mathbf{X}} = \{\tilde{X}_i\}_{i=1}^{1000}$ . We then compute the approximate likelihood,

$$\begin{aligned} \mathcal{L}(\theta) = P^4(200 \leq T(2n+1) \leq 450) &\cdot \left[ 1 - \right. \\ 346 \quad &P_{\tilde{\mathbf{X}}}^4(\{T(2n^*) < 1700\} \mid 200 \leq T(2n+1) \leq 450) - \\ &P_{\tilde{\mathbf{X}}}^4(\{1700 < T(2n^*) < 2350\} \mid 200 \leq T(2n+1) \leq 450) + \\ &\left. P_{\tilde{\mathbf{X}}}^4(\{T(2n^*) < 1700\} \wedge \{1700 < T(2n^*) < 2350\} \mid 200 \leq T(2n+1) \leq 450) \right], \end{aligned} \quad (4)$$

where  $!\{\dots\}$  is the "logical not" operator,  $P^4(\dots)$  is the 4th power of  $P(\dots)$ , and all probabilities

348  $P_{\tilde{\mathbf{X}}}(\dots)$  are approximated from the results of the simulations  $\tilde{\mathbf{X}}$ . For example,  $P_{\tilde{\mathbf{X}}}(\{T(2n^*) < 1700\} \mid$

200  $\leq T(2n+1) \leq 450$ ) is approximated by taking simulations in which  $2n+1$  fixed (reached >95%)

350 before generation 450 but not before generation 200, and computing the fraction of such simulations

in which  $2n^*$  did not fix by generation 1,700, and hence aneuploidy did not extinct (reach <5%)

352 before generation 1,700. Figure S1 compares results with less and more simulated experiments,

demonstrating that 1,000 simulations are likely sufficient.

354 For a model without aneuploidy (that is, when the aneuploidy rate is fixed at zero,  $\delta = 0$ ), we disregard

the increased expression in Chromosome III and the growth advantage measured in generation 450,

356 and focus on the growth advantage measured in later generations, presumably due to a beneficial

mutation. Therefore, the likelihood is approximated by

$$\begin{aligned} \mathcal{L}_!(\theta) = 1 - P_{\tilde{\mathbf{X}}}^4(\{T(2n^*) < 1700\}) - \\ 358 \quad P_{\tilde{\mathbf{X}}}^4(\{1700 < T(2n^*) < 2350\}) + \\ &P_{\tilde{\mathbf{X}}}^4(\{T(2n^*) < 1700\} \wedge \{1700 < T(2n^*) < 2350\}). \end{aligned} \quad (5)$$

**Parameter inference.** To infer model parameters, we use approximate Bayesian computation with

360 a sequential Monte-Carlo scheme, or ABC-SMC (Sisson et al., 2007), implemented in the pyABC

Python package (Klinger et al., 2018, [pyabc.readthedocs.io](https://pyabc.readthedocs.io)). This approach uses numerical stochastic

362 simulations of the model to infer a posterior distribution over the model parameters. It is a method of

likelihood-free, simulation-based inference (Cranmer et al., 2020), that is, for estimating a posterior

364 distribution when a likelihood function cannot be directly computed. It is therefore suitable in our

case, in which the likelihood function can only be approximated from simulations, and cannot be

366 directly computed.

The ABC-SMC algorithm employs sequential importance sampling over multiple iterations (Toni

368 et al., 2009; Klinger and Hasenauer, 2017; Syga et al., 2021). In iteration  $t$  of the algorithm, a

set of parameter vectors,  $\{\theta_{i,t}\}_{i=1}^{n_t}$ , also called *particles*, are constructed in the following way. A

370 proposal particle,  $\theta^*$ , is sampled from a proposal distribution, and is either accepted or rejected, until

$n_t$  particles are accepted. The number of particles,  $n_t$ , is adapted at every iteration  $t$  using the adaptive population strategy (Klinger et al., 2018, [pyabc.readthedocs.io](https://pyabc.readthedocs.io)). For  $t = 0$ , the proposal particle is sampled from the prior distribution,  $p(\theta)$ . For  $t > 0$ , the proposal particle is sampled from the particles accepted in the previous iteration,  $\{\theta_{i,t-1}\}_{i=1}^{n_{t-1}}$ , each with a probability relative to its weight  $W_{t-1}(\theta_{i,t-1})$  (see below). The proposal particle is then perturbed using a kernel perturbation kernel,  $K_t(\theta^* | \theta)$  where  $\theta$  is the sample from the previous iteration. Then, a set of synthetic observations  $\tilde{\mathbf{X}}^*$  is simulated, and the proposal particle  $\theta^*$  is accepted if its approximate likelihood (eq. (4)) is high enough,  $\mathcal{L}(\theta^*) > 1 - \epsilon_t$  (or more commonly, if  $1 - \mathcal{L}(\theta^*) < \epsilon_t$ ), where  $\epsilon_t > 0$  is the *acceptance threshold*, as higher values of  $\epsilon_t$  allow more particles to be accepted. The acceptance threshold  $\epsilon_t$  is chosen as the median of the  $1 - \mathcal{L}(\theta)$  of the particles accepted in the previous iteration,  $t - 1$ , and  $\epsilon_0 = 0.01$ . For each accepted particle  $\theta_{i,t}$  a weight  $W_t(\theta_{i,t})$  is assigned: for  $t = 0$ ,  $W_0(\theta_{i,0}) = 1$ , and for  $t > 0$ ,  $W_t(\theta_{i,t}) = p(\theta_{i,t}) / \sum_{i=1}^{n_{t-1}} W_{t-1}(\theta_{i,t-1}) K_t(\theta_{i,t}, \theta_{i,t-1})$ , where  $p(\theta)$  is the prior density of  $\theta$  and  $K_t(\theta', \theta)$  is the probability of a perturbation from  $\theta$  to  $\theta'$ .  $K_t(\theta' | \theta)$  is a multivariate normal distribution, fitted at iteration  $t$  to the particles from the previous iteration,  $\{\theta_{i,t-1}\}_{i=1}^{n_{t-1}}$ , and their weights,  $\{W(\theta_{i,t-1})\}_{i=1}^{n_{t-1}}$ .

Acceptance is determined according to the approximate likelihood (eq. (4)), which has a maximum value of  $\mathcal{L}_{max} = 0.875$  (giving a minimal value of  $\epsilon_{min} = 0.125$ ). We terminated the inference iterations when the change in  $\epsilon$  value from one iteration to the next was small. With our standard prior and model, we reached  $\epsilon = 0.13$  (or  $\mathcal{L} = 0.87$ ) after six iterations, with  $n_6 = 982$  accepted parameter vectors and effective sample size ESS=651 (Figure S2). Running the inference algorithm with different initialization seeds and less or more simulations for approximating the likelihood produced similar posterior distributions (Figure S1).

After producing a set of weighted particles from the the posterior distribution using the above ABC-SMC algorithm, we approximate the posterior using kernel density estimation (KDE) with Gaussian kernels. We truncate the estimated posterior to avoid positive posterior density for values with zero prior density. The MAP (maximum a posteriori) estimate is computed as the the maximum of the estimated joint posterior density. We then draw 5,000,000 samples from the posterior distribution to compute the HDI (highest density interval) and draw 50,000 samples to visualize the posterior distribution with histograms.

**Model comparison.** We examine several versions of our evolutionary models, e.g. without aneuploidy or with increased mutation rate in aneuploid cells, as well as several different prior distributions (see below). To compare these, we plot posterior predictions: for each model we execute 10,000

simulations using the MAP parameter estimates and plot the distributions of time to fixation of  $2n^*$ ,  
404 one of key properties of the model likelihood. These plots visualize the fit of each model to the  
data. Also, for similar models we plot the marginal and joint posterior distributions of the parameters;  
406 if these are similar, we consider the models interchangeable. We validate this by comparing HDI  
(highest density interval) of posterior distributions.

408 Where posterior plots are very similar and the number of parameters is the same, we use WAIC, or  
the widely applicable information criterion (Gelman et al., 2013), defined as

410 
$$WAIC(\theta) = -2 \log \mathbb{E}[\mathcal{L}(\theta)] + 2\mathbb{V}[\log \mathcal{L}(\theta)] \quad (6)$$

where  $\theta$  is a parameter vector, and  $\mathbb{E}[\cdot]$  and  $\mathbb{V}[\cdot]$  are the expectation and variance taken over the  
412 posterior distribution, which in practice are approximated using 50,000 samples from the posterior  
KDE. We validated that upon resampling WAIC values do not significantly change and that differences  
414 in WAIC between models are preserved. WAIC values are scaled as a deviance measure: lower values  
imply higher predictive accuracy.

416 **Prior distributions.** We used informative prior distributions for  $w_{2n+1}$ ,  $w_{2n+1^*}$  and  $w_{2n^*}$  (we set  
 $w_{2n} = 1$ ), which we estimated from growth curves data from mono-culture growth experiments pre-  
418 viously reported by Yona et al. (2012, Figs. 3C, 4A, and S2). We used Curveball, a method  
for predicting results of competition experiments from growth curve data (Ram et al., 2019, [curve-  
420 ball.yoavram.com](http://curveball.yoavram.com)). Briefly, Curveball takes growth curves of two strains growing separately in  
mono-culture and predicts how they would grow in a mixed culture, that is, it predicts the results  
422 of a competition assay. From these predictions, relative fitness values can be computed. Because  
Curveball uses a maximum-likelihood approach to estimate model parameters, we were able to  
424 estimate a distribution of relative fitness values to be used as a prior distribution by sampling 10,000  
samples from a truncated multivariate normal distribution defined by the maximum-likelihood covari-  
426 ance matrix (Figure S3).

We used growth curves of  $2n$  and  $2n + 1$  in 39°C to estimate an informative prior distribution for  
428  $w_{2n+1}$  (Figure S3D, assuming  $w_{2n} = 1$ ). In this prior distribution, we used the same prior for  $w_{2n+1^*}$   
and  $w_{2n^*}$ . To increase computational efficiency, we also assumed  $w_{2n^*} > w_{2n+1^*} > w_{2n+1} > w_{2n}$ ;  
430 running the inference without this assumption produced similar results. See *supporting material* for  
an extended informative prior distribution that uses growth curves of  $2n^*$  and  $2n + 1$  growing in 39°C;  
432 this prior distribution proved to be less useful.

As a control, we tested an uninformative uniform prior with  $U(1, 6)$ , for (i) all  $w_{2n+1}$ ,  $w_{2n+1^*}$ ,  $w_{2n^*}$ ,

- 434 or (ii) only for  $w_{2n+1^*}$ ,  $w_{2n^*}$ , using the above informative prior for  $w_{2n+1}$ . In these cases the inference  
algorithm failed to converge.
- 436 For the mutation rate,  $\mu$ , and aneuploidy rate,  $\delta$ , we used uninformative uniform priors,  $\mu \sim U(10^{-9}, 10^{-5})$  and  $\delta \sim U(10^{-6}, 10^{-2})$ . A wider mutation rate prior,  $\mu \sim U(10^{-9}, 10^{-3})$ , produced  
438 similar results.

## Acknowledgements

- 440 We thank Lilach Hadany, Judith Berman, David Gresham, Shay Covo, Martin Kupiec, Uri Obolski, Daniel  
Weissman, and Tal Simon for discussions and comments. This work was supported in part by the Israel Science  
442 Foundation (ISF, YR 552/19), the US–Israel Binational Science Foundation (BSF, YR 2021276), Minerva  
Center for Live Emulation of Evolution in the Lab (YR, YP), Minerva Stiftung short-term research grant (MP),  
444 the Burroughs Wellcome Fund (AS), and the Jane Coffin Childs Memorial Fund (PVZ).

## References

- 446 Avecilla, G., Chuong, J. N., Li, F., Sherlock, G., Gresham, D. and Ram, Y. (2022), ‘Neural networks  
enable efficient and accurate simulation-based inference of evolutionary parameters from adaptation  
448 dynamics’, *PLOS Biology* **20**(5), e3001633.
- 450 Avecilla, G., Spealman, P., Matthews, J., Caudal, E., Schacherer, J. and Gresham, D. (2023), ‘Copy  
number variation alters local and global mutational tolerance’, *Genome Research* .
- 452 Bakhoum, S. F. and Landau, D. A. (2017), ‘Chromosomal instability as a driver of tumor heterogeneity  
and evolution’, *Cold Spring Harb. Perspect. Med.* **7**(6), 1–14.
- 454 Barney, J. B., Chandrashekappa, D. G., Soncini, S. R. and Schmidt, M. C. (2021), ‘Drug resistance  
in diploid yeast is acquired through dominant alleles, haploinsufficiency, gene duplication and  
aneuploidy’, *PLOS Genetics* **17**(9).
- 456 Bouchonville, K., Forche, A., Tang, K. E. S., Semple, C. a. M. and Berman, J. (2009), ‘Aneuploid  
chromosomes are highly unstable during dna transformation of *Candida albicans*.’, *Eukaryot. Cell*  
458 **8**(10), 1554–66.
- Boveri, T. (2008), ‘Concerning the origin of malignant tumours’, *J. Cell Sci.* **121**(Supplement 1), 1–84.
- 460 Chen, G., Bradford, W. D., Seidel, C. W. and Li, R. (2012), ‘Hsp90 stress potentiates rapid cellular  
adaptation through induction of aneuploidy.’, *Nature* **482**(7384), 246–50.

- 462 Chen, G., Rubinstein, B. and Li, R. (2012), ‘Whole chromosome aneuploidy: Big mutations drive  
adaptation by phenotypic leap’, *BioEssays* **34**(10), 893–900.
- 464 Covo, S., Puccia, C. M., Argueso, J. L., Gordenin, D. A. and Resnick, M. A. (2014), ‘The sister chro-  
matid cohesion pathway suppresses multiple chromosome gain and chromosome amplification.’,  
466 *Genetics* **196**(2), 373–384.
- 468 Cranmer, K., Brehmer, J. and Louppe, G. (2020), ‘The frontier of simulation-based inference’, *Pro-  
ceedings of the National Academy of Sciences* p. 201912789.
- 470 Crow, J. F. and Kimura, M. (1970), *An introduction to population genetics theory*, Burgess Pub. Co.,  
Minneapolis.
- 472 Dhar, R., Sägesser, R., Weikert, C., Yuan, J. and Wagner, A. (2011), ‘Adaptation of *Saccharomyces  
cerevisiae* to saline stress through laboratory evolution.’, *J. Evol. Biol.* **24**(5), 1135–53.
- 474 Dunham, M. J., Badrane, H., Ferea, T., Adams, J., Brown, P. O., Rosenzweig, F. and Botstein,  
D. (2002), ‘Characteristic genome rearrangements in experimental evolution of *Saccharomyces  
cerevisiae*’, *Proc. Natl. Acad. Sci.* **99**(25), 16144–16149.
- 476 Elde, Nels, C., Child, Stephanie, J., Eickbush, Michael, T., Kitzman, Jacob, O., Rogers, Kelsey,  
S., Shendure, J., Geballe, Adam, P. and Malik, Harmit, S. (2012), ‘Poxviruses deploy genomic  
478 accordions to adapt rapidly against host antiviral defenses’, *Cell* **150**(4), 831–841.
- 480 Flynn, J. M., Rossouw, A., Cote-Hammarlof, P., Fragata, I., Mavor, D., Hollins, C., Bank, C. and Bolon,  
D. N. (2020), ‘Comprehensive fitness maps of hsp90 show widespread environmental dependence’,  
*Elife* **9**, 1–25.
- 482 Gelman, A., Carlin, J. B., Stern, H. S., Dunson, D. B., Vehtari, A. and Rubin, D. B. (2013), *Bayesian  
Data Analysis, Third Edition*, Chapman & Hall/CRC Texts in Statistical Science, Taylor & Francis.
- 484 Gerstein, A. C. and Berman, J. (2020), ‘*Candida albicans* genetic background influences mean and  
heterogeneity of drug responses and genome stability during evolution in fluconazole’, *mSphere*  
486 **5**(3).
- 488 Gerstein, A. C., Ono, J., Lo, D. S., Campbell, M. L., Kuzmin, A. and Otto, S. P. (2015), ‘Too much of  
a good thing: the unique and repeated paths toward copper adaptation.’, *Genetics* **199**(2), 555–71.
- 490 Gilchrist, C. and Stelkens, R. (2019), ‘Aneuploidy in yeast: Segregation error or adaptation mecha-  
nism?’, *Yeast* **36**(9), 525–539.
- Good, B. H., Rouzine, I. M., Balick, D. J., Hallatschek, O. and Desai, M. M. (2012), ‘Distribution

- 492 of fixed beneficial mutations and the rate of adaptation in asexual populations.', *Proceedings of the National Academy of Sciences* .
- 494 Gresham, D., Desai, M. M., Tucker, C. M., Jenq, H. T., Pai, D. A., Ward, A., DeSevo, C. G.,  
496 Botstein, D. and Dunham, M. J. (2008), 'The repertoire and dynamics of evolutionary adaptations to controlled nutrient-limited environments in yeast', *PLoS Genet.* **4**(12).
- Heidenreich, E. (2007), 'Adaptive Mutation in *Saccharomyces cerevisiae*', *Crit. Rev. Biochem. Mol. Biol.* **42**(4), 285–311.
- Hong, J. and Gresham, D. (2014), 'Molecular specificity, convergence and constraint shape adaptive evolution in nutrient-poor environments', *PLoS Genet.* **10**(1).
- Huang, C. J., Lu, M. Y., Chang, Y. W. and Li, W. H. (2018), 'Experimental Evolution of Yeast for High-Temperature Tolerance', *Mol. Biol. Evol.* **35**(8), 1823–1839.
- Ippolito, M. R., Martis, V., Martin, S., Tijhuis, A. E., Hong, C., Wardenaar, R., Dumont, M., Zerbib,  
504 J., Spierings, D. C., Fachinetti, D., Ben-David, U., Foijer, F. and Santaguida, S. (2021), 'Gene copy-number changes and chromosomal instability induced by aneuploidy confer resistance to  
506 chemotherapy', *Dev. Cell* **56**(17), 2440–2454.e6.
- Iwasa, Y., Michor, F. and Nowak, M. A. (2004), 'Stochastic tunnels in evolutionary dynamics', *Genetics* **166**(3), 1571–1579.
- Jarolim, S., Ayer, A., Pillay, B., Gee, A. C., Phrakaysone, A., Perrone, G. G., Breitenbach, M. and Dawes, I. W. (2013), 'Saccharomyces cerevisiae genes involved in survival of heat shock', *G3 Genes, Genomes, Genetics* **3**(12), 2321–2333.
- Kasuga, T., Bui, M., Bernhardt, E., Swiecki, T., Aram, K., Cano, L. M., Webber, J., Brasier, C., Press, C., Grünwald, N. J., Rizzo, D. M. and Garbelotto, M. (2016), 'Host-induced aneuploidy and phenotypic diversification in the sudden oak death pathogen *Phytophthora ramorum*', *BMC Genomics* **17**(1), 1–17.
- Klinger, E. and Hasenauer, J. (2017), A scheme for adaptive selection of population sizes in approximate bayesian computation - sequential monte carlo, *in* J. Feret and H. Koeppl, eds, 'Computational Methods in Systems Biology', Vol. 10545, Springer International Publishing, pp. 128–144. Series Title: Lecture Notes in Computer Science.
- Klinger, E., Rickert, D. and Hasenauer, J. (2018), 'pyabc: distributed, likelihood-free inference', *Bioinformatics* (May), 1–3.

- 522 Kohn, L. M. and Anderson, J. B. (2014), ‘The underlying structure of adaptation under strong selection  
in 12 experimental yeast populations’, *Eukaryot. Cell* **13**(9), 1200–1206.
- 524 Komarova, N. L., Sengupta, A. and Nowak, M. A. (2003), ‘Mutation-selection networks of cancer  
initiation: Tumor suppressor genes and chromosomal instability’, *Journal of Theoretical Biology*  
526 **223**(4), 433–450.
- Kronholm, I. and Collins, S. (2016), ‘Epigenetic mutations can both help and hinder adaptive evolu-  
528 tion’, *Molecular Ecology* **25**(8), 1856–1868.
- Kumaran, R., Yang, S.-Y. and Leu, J.-Y. (2013), ‘Characterization of chromosome stability in diploid,  
530 polyplloid and hybrid yeast cells’, *PLoS ONE* **8**(7), e68094.
- Lauer, S., Avecilla, G., Spealman, P., Sethia, G., Brandt, N., Levy, S. F. and Gresham, D. (2018),  
532 ‘Single-cell copy number variant detection reveals the dynamics and diversity of adaptation.’, *PLOS  
Biology* **16**.
- 534 Lukow, D. A., Sausville, E. L., Suri, P., Chunduri, N. K., Wieland, A., Leu, J., Smith, J. C., Girish,  
V., Kumar, A. A., Kendall, J., Wang, Z., Storchova, Z. and Sheltzer, J. M. (2021), ‘Chromosomal  
536 instability accelerates the evolution of resistance to anti-cancer therapies’, *Developmental Cell*  
**56**(17), 2427–2439.e4.
- 538 Lynch, M., Sung, W., Morris, K., Coffey, N., Landry, C. R., Dopman, E. B., Dickinson, W. J.,  
Okamoto, K., Kulkarni, S., Hartl, D. L. and Thomas, W. K. (2008), ‘A genome-wide view of the  
540 spectrum of spontaneous mutations in yeast’, *Proceedings of the National Academy of Sciences*  
**105**(27), 9272–9277.
- 542 Mannaert, A., Downing, T., Imamura, H. and Dujardin, J. C. (2012), ‘Adaptive mechanisms in  
pathogens: Universal aneuploidy in *Leishmania*’, *Trends Parasitol.* **28**(9), 370–376.
- 544 Möller, M., Habig, M., Freitag, M. and Stukenbrock, E. H. (2018), ‘Extraordinary genome instability  
and widespread chromosome rearrangements during vegetative growth’, *Genetics* **210**(2), 517–529.
- 546 Naylor, R. M. and van Deursen, J. M. (2016), ‘Aneuploidy in cancer and aging’, *Annu. Rev. Genet.*  
**50**(1), 45–66.
- 548 Niwa, O., Tange, Y. and Kurabayashi, A. (2006), ‘Growth arrest and chromosome instability in  
aneuploid yeast’, *Yeast* **23**(13), 937–950.
- 550 Otto, S. P. and Day, T. (2007), *A biologist’s guide to mathematical modeling in ecology and evolution*,  
Princeton University Press.

- 552 Pavelka, N., Rancati, G., Zhu, J., Bradford, W. D., Saraf, A., Florens, L., Sanderson, B. W., Hattem,  
G. L. and Li, R. (2010), ‘Aneuploidy confers quantitative proteome changes and phenotypic variation  
554 in budding yeast.’, *Nature* **468**(7321), 321–5.
- Peter, J., De Chiara, M., Friedrich, A., Yue, J. X., Pflieger, D., Bergström, A., Sigwalt, A., Barre, B.,  
556 Freel, K., Llored, A., Cruaud, C., Labadie, K., Aury, J. M., Istance, B., Lebrigand, K., Barbry, P.,  
Engelen, S., Lemainque, A., Wincker, P., Liti, G. and Schacherer, J. (2018), ‘Genome evolution  
558 across 1,011 *Saccharomyces cerevisiae* isolates’, *Nature* **556**(7701), 339–344.
- Ram, Y., Dellus-Gur, E., Bibi, M., Karkare, K., Obolski, U., Feldman, M. W., Cooper, T. F., Berman,  
560 J. and Hadany, L. (2019), ‘Predicting microbial growth in a mixed culture from growth curve data’,  
*Proceedings of the National Academy of Sciences* **116**(29), 14698–14707.
- 562 Rancati, G., Pavelka, N., Fleharty, B., Noll, A., Trimble, R., Walton, K., Perera, A., Staehling-  
Hampton, K., Seidel, C. W. and Li, R. (2008), ‘Aneuploidy underlies rapid adaptive evolution of  
564 yeast cells deprived of a conserved cytokinesis motor’, *Cell* **135**(5), 879–893.
- Robbins, N., Caplan, T. and Cowen, L. E. (2017), ‘Molecular evolution of antifungal drug resistance’,  
566 *Annu. Rev. Microbiol.* **71**(1), 753–775.
- Robinson, D., Vanacloig-Pedros, E., Cai, R., Place, M., Hose, J. and Gasch, A. P. (2023), ‘Gene-by-  
568 environment interactions influence the fitness cost of gene copy-number variation in yeast’, *bioRxiv*
- .
- 570 Rodrigues, M. L. and Albuquerque, P. C. (2018), ‘Searching for a change: The need for increased  
support for public health and research on fungal diseases’, *PLoS Negl. Trop. Dis.* **12**(6), 1–5.
- 572 Rutledge, S. D., Douglas, T. A., Nicholson, J. M., Vila-Casadesús, M., Kantzler, C. L., Wangsa, D.,  
Barroso-Vilares, M., Kale, S. D., Logarinho, E. and Cimini, D. (2016), ‘Selective advantage of  
574 trisomic human cells cultured in non-standard conditions’, *Scientific Reports* **6**(June 2015), 1–12.
- Santaguida, S. and Amon, A. (2015), ‘Short- and long-term effects of chromosome mis-segregation  
576 and aneuploidy’, *Nat. Rev. Mol. Cell Biol.* **16**(8), 473–485.
- Santaguida, S., Vasile, E., White, E. and Amon, A. (2015), ‘Aneuploidy-induced cellular stresses limit  
578 autophagic degradation’, *Genes Dev.* **29**(19), 2010–2021.
- Schvartzman, J. M., Sotillo, R. and Benezra, R. (2010), ‘Mitotic chromosomal instability and cancer:  
580 Mouse modelling of the human disease’, *Nat. Rev. Cancer* **10**(2), 102–115.
- Selmecki, A. M., Dulmage, K., Cowen, L. E., Anderson, J. B. and Berman, J. (2009), ‘Acquisition

- 582 of aneuploidy provides increased fitness during the evolution of antifungal drug resistance', *PLoS Genet.* **5**(10), e1000705.
- 584 Selmecki, A. M., Forche, A. and Berman, J. (2010), 'Genomic plasticity of the human fungal pathogen *Candida albicans*', *Eukaryot. Cell* **9**(7), 991–1008.
- 586 Selmecki, A. M., Gerami-Nejad, M., Paulson, C., Forche, A. and Berman, J. (2008), 'An isochromosome confers drug resistance in vivo by amplification of two genes, erg11 and tac1', *Mol. Microbiol.*
- 588 **68**(3), 624–641.
- 590 Sheltzer, J. M. and Amon, A. (2011), 'The aneuploidy paradox: Costs and benefits of an incorrect karyotype', *Trends Genet.* **27**(11), 446–453.
- 592 Sheltzer, J. M., Blank, H. M., Pfau, S. J., Tange, Y., George, B. M., Humpton, T. J., Brito, I. L., Hiraoka, Y., Niwa, O. and Amon, A. (2011), 'Aneuploidy drives genomic instability in yeast', *Science* **333**(6045), 1026–1030.
- 594 Sheltzer, J. M., Ko, J. H., Replogle, J. M., Habibe Burgos, N. C., Chung, E. S., Meehl, C. M., Sayles, N. M., Passerini, V., Storchova, Z. and Amon, A. (2017), 'Single-chromosome gains commonly function as tumor suppressors', *Cancer Cell* **31**(2), 240–255.
- 598 Sionov, E., Lee, H., Chang, Y. C. and Kwon-Chung, K. J. (2010), '*Cryptococcus neoformans* overcomes stress of azole drugs by formation of disomy in specific multiple chromosomes', *PLoS Pathog.* **6**(4), e1000848.
- 600 Sisson, S. A., Fan, Y. and Tanaka, M. M. (2007), 'Sequential monte carlo without likelihoods', *Proceedings of the National Academy of Sciences* **104**(6), 1760–1765.
- 602 Soncini, S. R., Chandrashekappa, D. G., Augustine, D. A., Callahan, K. P., O'Donnell, A. F. and Schmidt, M. C. (2020), 'Spontaneous mutations that confer resistance to 2-deoxyglucose act through Hxk2 and Snf1 pathways to regulate gene expression and HXT endocytosis', *PLOS Genetics* **16**(7).
- 604 Sonti, R. V. and Roth, J. R. (1989), 'Role of gene duplications in the adaptation of *Salmonella typhimurium* to growth on limiting carbon sources.', *Genetics* **123**(1), 19–28.
- 608 Syga, S., David-Rus, D., Schälte, Y., Hatzikirou, H. and Deutsch, A. (2021), 'Inferring the effect of interventions on covid-19 transmission networks', *Scientific Reports* **11**(1), 1–11.
- 610 Todd, R. T., Forche, A. and Selmecki, A. M. (2017), 'Ploidy variation in fungi: Polyploidy, aneuploidy, and genome evolution', *Microbiol. Spectr.* **5**(4), 1–20.
- Toni, T., Welch, D., Strelkowa, N., Ipsen, A. and Stumpf, M. P. (2009), 'Approximate bayesian

- 612 computation scheme for parameter inference and model selection in dynamical systems', *J. R. Soc. Interface* **6**(31), 187–202.
- 614 Torres, E. M., Dephoure, N., Panneerselvam, A., Tucker, C. M., Whittaker, C. A., Gygi, S. P., Dunham, M. J. and Amon, A. (2010), 'Identification of aneuploidy-tolerating mutations', *Cell* **143**(1), 71–83.
- 616 Torres, E. M., Sokolsky, T., Tucker, C. M., Chan, L. Y., Boselli, M., Dunham, M. J. and Amon, A. (2007), 'Effects of aneuploidy on cellular physiology and cell division in haploid yeast', *Science* 618 (80-). **317**(5840), 916–924.
- 620 Tsai, H. J., Nelliat, A. R., Choudhury, M. I., Kucharavy, A., Bradford, W. D., Cook, M. E., Kim, J., Mair, D. B., Sun, S. X., Schatz, M. C. and Li, R. (2019), 'Hypo-osmotic-like stress underlies general cellular defects of aneuploidy', *Nature* .
- 622 Williams, B. R., Prabhu, V. R., Hunter, K. E., Glazier, C. M., Whittaker, C. a., Housman, D. E. and Amon, A. (2008), 'Aneuploidy affects proliferation and spontaneous immortalization in mammalian cells', *Science* **322**(5902), 703–709.
- 624 Yang, F., Todd, R. T., Selmecki, A., Jiang, Y. Y., Cao, Y. B. and Berman, J. (2021), 'The fitness costs and benefits of trisomy of each *Candida albicans* chromosome', *Genetics* **218**(2), 1–7.
- 626 Yona, A. H., Frumkin, I. and Pilpel, Y. (2015), 'A relay race on the evolutionary adaptation spectrum', *Cell* **163**(3), 549–559.
- 630 Yona, A. H., Manor, Y. S., Herbst, R. H., Romano, G. H., Mitchell, A., Kupiec, M., Pilpel, Y. and Dahan, O. (2012), 'Chromosomal duplication is a transient evolutionary solution to stress.', *Proceedings of the National Academy of Sciences* **109**(51), 21010–5.
- 632 Zhu, J., Pavelka, N., Bradford, W. D., Rancati, G. and Li, R. (2012), 'Karyotypic determinants of chromosome instability in aneuploid budding yeast', *PLoS Genetics* **8**(5).
- 634 Zhu, J., Tsai, H.-J., Gordon, M. R. and Li, R. (2018), 'Cellular stress associated with aneuploidy', *Dev. Cell* **44**(4), 420–431.
- 636 Zhu, Y. O., Sherlock, G. and Petrov, D. A. (2016), 'Whole genome analysis of 132 clinical *Saccharomyces cerevisiae* strains reveals extensive ploidy variation', *G3 Genes, Genomes, Genetics* 638 **6**(8), 2421–2434.
- Zhu, Y. O., Siegal, M. L., Hall, D. W. and Petrov, D. A. (2014), 'Precise estimates of mutation rate and spectrum in yeast', *Proceedings of the National Academy of Sciences* **111**(22), E2310–E2318.